B. Bouhadouza, F. Sadaoui

Optimal power flow analysis under photovoltaic and wind power uncertainties using the blood-sucking leech optimizer

Introduction. Optimal power flow (OPF) is a fundamental task in modern power systems, aiming to ensure cost-effective generation dispatch and efficient energy distribution. The increasing integration of renewable energy sources such as photovoltaic (PV) and wind turbines (WT), alongside conventional thermal units, introduces significant variability and uncertainty into system operations. Problem. The OPF problem is nonlinear, constrained by complex technical limits, and further complicated by the stochastic nature of PV and WT power generation. Efficiently addressing these uncertainties while maintaining system optimality remains a major challenge. The goal of this study is to solve the OPF problem in power networks that integrate PV and WT systems, while accounting for the uncertainty in their power outputs. Methodology. The stochastic behavior of PV and WT units is modeled using probability distribution functions. A novel bio-inspired metaheuristic, the Blood-Sucking Leech Optimizer (BSLO), is proposed and benchmarked against two well-established algorithms: Particle Swarm Optimization (PSO) and Grey Wolf Optimizer (GWO). Simulations are conducted on both the IEEE 30-bus test system and a real Algerian transmission network. Results. The BSLO algorithm consistently outperforms PSO and GWO in minimizing generation cost, power losses, and voltage deviation across all tested scenarios. Scientific novelty. This work considers both single and multi-objective OPF formulations, whereas most previous studies focus solely on single-objective approaches. It integrates renewable generation uncertainty through probabilistic modeling and introduces a novel metaheuristic (BSLO). Validation on a real Algerian power grid confirms the method's robustness and practical relevance. Practical value. The results confirm the BSLO algorithm as a promising and effective tool for solving complex, renewable-integrated OPF problems in real-world power systems, contributing to more reliable, economical, and flexible grid operation. References 48, tables 13, figures 17.

Key words: blood-sucking leech optimizer, optimal power flow, stochastic renewable energy sources, power systems.

Вступ. Оптимальний розподіл потужності (OPF) ϵ фундаментальним завданням у сучасних енергосистемах, спрямованим на забезпечення економічно ефективного розподілу та генерації енергії. Зростаюча інтеграція відновлюваних джерел енергії, таких як фотоелектричні (PV) та вітрові турбіни (WT), поряд з традиційними тепловими установками, вносить значну мінливість та невизначеність у роботу системи. **Проблема**. Завдання OPF ϵ нелінійним зі складними технічними обмеженнями та додатково ускладненим стохастичною природою генерації електроенергії РV та WT установками. Ефективне вирішення ших невизначеностей за збереження оптимальності системи залишається серйозною проблемою. **Метою** роботи є вирішення завдання *OPF* в енергомережах з інтегрованими PV та WT системами з урахуванням невизначеності їхньої вихідної потужності. Методика. Стохастична поведінка PV та WT установок моделюється з використанням функцій розподілу ймовірностей. Запропоновано новий біоінспірований метаевристичний алгоритм на основі поведінки п'явки (BSLO), який порівнюється з двома алгоритмами, що добре зарекомендували себе: метод рою частинок (PSO) і метод сірого вовка (GWO). Моделювання проводилося як у тестовій системі IEEE з 30 шинами, так і у реальній алжирській мережі електропередачі. Результати. Алгоритм BSLO стабільно перевершує PSO та GWO щодо мінімізації вартості генерації, втрат потужності та відхилень напруги у всіх протестованих сценаріях. Наукова новизна. У цій роботі розглядаються як однокритеріальні, так і багатокритеріальні формулювання ОРГ, тоді як більшість попередніх досліджень фокусувалися виключно на однокритеріальних підходах. Це враховує невизначеність генерації відновлюваних джерел енергії за допомогою імовірнісного моделювання і представляє новий метаевристичний алгоритм (BSLO). Перевірка на реальній алжирській енергосистемі підтверджує надійність та практичну значущість методу. **Практична значимість**. Результати підтверджують, що алгоритм BSLO є перспективним та ефективним інструментом для вирішення складних завдань ОРГ, інтегрованих з відновлюваними джерелами енергії, у реальних енергосистемах, сприяючи більш надійній, економічній та гнучкішій роботі мережі. Бібл. 48, табл. 13, рис. 17.

Ключові слова: оптимізатор на основі поведінки п'явки, оптимальний розподіл потужності, стохастичні відновлювані джерела енергії, енергетичні системи.

Introduction. Power flow analysis is the essential tool used to assess the performance of electrical networks. It focuses on several key parameters, including voltage profiles, line power flows, the balance between generation and load powers, and losses. In contrast, optimal power flow (OPF) analysis plays a critical role in the design and operational planning of electrical grids. OPF helps identify potential design weaknesses, improves the reliability of energy supply, and ensures efficient system operation [1–3]. The main goal of OPF is to define the best set of decision variables that optimize a predefined objective function. One of its most common applications is the economic dispatch of power supply, aiming to minimize the overall generation cost and satisfy operational and safety constraints [4–10].

Conventionally, power generation has relied heavily on fossil fuel-based thermal units. However, the integration of photovoltaic (PV) and wind turbines (WT) generators offers considerable benefits, reduced greenhouse gas emissions and decreased dependence on fossil fuels [11, 12]. Despite these advantages, renewable energy sources introduce new challenges due to their power uncertainty. Indeed, the power generation of PV and WT systems is highly dependent on changing weather conditions, specifically wind speed and solar irradiance. Therefore, it is essential to address the OPF problem while considering the stochastic nature of renewable energy generation to maintain grid stability and achieve economic efficiency [13, 14].

Traditional methods for solving OPF problems, such as the Newton-based method, linear and nonlinear programming, and others [15–20], often struggle to converge to the global optimum. This limitation stems from the highly nonlinear, non-convex, and complex form of the power system equations, and the presence of multiple operational constraints. Consequently, conventional optimization techniques may fail to provide reliable or accurate solutions for large-scale or modernized power grids. To address these challenges, researchers have

© B. Bouhadouza, F. Sadaoui

increasingly turned to advanced optimization strategies, particularly metaheuristic algorithms, which have gained significant attention in recent decades for their robustness and flexibility in handling complex and multi-objective OPF problems [21–23].

Metaheuristic algorithms, including standard, improved, and hybrid variants, are widely employed to address complex, non-linear, and high-dimensional optimization challenges in power systems, such as OPF problem, unit commitment, and renewable energy integration. These methods overcome the limitations of traditional approaches by efficiently exploring large search spaces and avoiding local optima. Standard metaheuristic algorithms are population-based and rely on stochastic search processes. Papers [24, 25] demonstrate the superiority of the Grey Wolf Optimizer (GWO) and Hamiltonian methods, respectively, in reducing power losses in electrical networks, compared to Particle Swarm Optimization (PSO) and Genetic Algorithms (GA). In [26], the author applies GWO to solve the OPF problem for different test systems, achieving lower generation costs compared to those obtained with GA and PSO. The authors in [27] introduce Differential Evolution (DE) to minimize cost, emissions, and real power losses in IEEE 30 and 118 bus systems, demonstrating improved performance over conventional methods.

The improved and hybrid methods are enhanced versions of standard metaheuristic algorithms, often combining 2 or more techniques to leverage their respective strengths. The authors in [28] improve the cuckoo optimization algorithm by incorporating a Gaussian mixture model, which improves convergence, accuracy, and robustness in systems with solar and wind sources. A stochastic optimization framework is presented in [29], combining probabilistic modeling with mathematical programming to handle renewable energy uncertainties and maintain system stability. In [30], a DE variant enhanced with fitness-distance balance adaptive guidance shows superior convergence efficiency. The paper [31] proposes a hybrid of the GWO and the crisscross search algorithm, which outperforms PSO, GA and DE algorithms.

The **goal** of the paper is to solve the OPF problem in power networks that integrate PV and WT systems; while accounting for the uncertainty in their power outputs. This uncertainty is modeled using probability distribution function (PDF) and the Monte Carlo simulation. 3 single-objective functions are considered: generation cost, active power losses and voltage deviation, as well as a multi-objective function combining these single objectives. The proposed approach, based on the Blood-Sucking Leech Optimizer (BSLO) algorithm, is evaluated on the standard IEEE 30-bus test system and in a real South-East Algerian Network (SEAN). The effectiveness of BSLO is assessed in terms of convergence characteristics, optimal solutions, and statistical indicators, and is compared to that of the PSO and GWO algorithms.

Problem formulation. The OPF problem consists in determining the optimal control variables that optimize an objective function and satisfy the system's constraints, and is formulated as follows:

$$\min F(x,u); \tag{1}$$

$$\begin{cases} g(x,u) = 0; \\ h(x,u) \le 0, \end{cases}$$
 (2)

where F is the OPF objective function; g, h are the equality and inequality constrains of the system.

The vector *x* contains all state variables, given by the following:

$$x = [P_{Th_1}, V_{L_1}, ..., V_{L_{NPQ}}, Q_{Th_1}, ..., Q_{Th_{NTh}}, ...$$

$$...Q_{WT_1}, ..., Q_{WT_{NWT}}, Q_{PV_1}, ..., Q_{PV_{NPV}}, S_{L_1}, ..., S_{L_{NL}}],$$
(3)

where P_{Th_1} is the real power generation of the slack generator; V_L is the voltage of the load bus; S_L is the apparent power in the transmission lines; Q_{Th} , Q_{WT} , Q_{PV} correspond to the reactive power outputs of thermal units, WT and PV systems, respectively; NL, NPQ, NWT, NPV, NTh indicate the number of transmission lines, load buses, WT, PV units and thermal plants, respectively.

The control variable vector *u* is defined as follows:

$$u = [P_{Th_2}, ..., P_{Th_{NTh}}, P_{WT_1}, ..., P_{WT_{NWT}}, ...$$

$$...P_{PV_1}, ..., P_{PV_{NPV}}, V_{G_1}, ..., V_{G_{NG}}],$$
(4)

where P_{Th} , P_{WT} , P_{PV} are the real powers generated by thermal generators, WT, and PV units, respectively; V_G is the voltage of the generation bus; N_G is the number of generators.

Fuel cost model of thermal generators. The total fuel cost of thermal generators is modeled using the following quadratic function [12, 23]:

$$F_{C1}(P_{Th}) = \sum_{i=1}^{NTh} a_i + b_i P_{Th_i} + c_i P_{Th_i}^2 , \qquad (5)$$

where a_i , b_i , c_i are the cost coefficients of the i^{th} generator.

For thermal units equipped with multi-valve steam turbines, the fuel cost model accounts for fluctuations in the cost function caused by the valve-point effect (VPE). This effect is modeled as a sinusoidal function integrated into the basic cost function, as shown in (5), yielding the total fuel cost (\$/h) [12, 32, 33]:

$$F_{C2}(P_{Th}) = \sum_{i=1}^{NTh} a_i + b_i P_{Th_i} + c_i P_{Th_i}^2 + \left| d_i \sin(e_i (P_{Th_i}^{\min} - P_{Th_i})) \right|, (6)$$

where d_i , e_i are the VPE coefficients.

Wind and solar's direct cost. Solar PV systems and WTs operate without requiring fuel, incurring only basic maintenance and operational costs. The direct cost model for PV and WT units is represented as a linear function of the planned power energy [12, 34]:

$$DC_{WT_i} = C_{DWT_i} P_{WTs_i}; (7)$$

$$DC_{PV_i} = C_{DPV_i} P_{PVs_i} , \qquad (8)$$

where P_{PVs_i} , P_{WTs_i} are the planned powers from the i^{th} PV and WT units; C_{DPV_i} , C_{DWT_i} are the direct cost coefficients for the i^{th} PV and WT generators.

Uncertainty of WTs and PVs cost functions. Depending on the power generated by the WTs, 2 scenarios can arise. If the generated power exceeds the planned power, an overestimation cost is applied. Conversely, if the generated power is lower than the planned power, an underestimation cost is applied. The expressions for these costs for the *i*th WT are formulated as follows [12, 34]:

$$UC_{WT_{i}} = C_{UWT_{i}}(P_{WTa_{i}} - P_{WTs_{i}}) =$$

$$= C_{UWT_{i}} \int_{P_{WTs_{i}}} (P_{WT_{i}} - P_{WTs_{i}}) f_{WT}(P_{WT_{i}}) dP_{WT_{i}};$$

$$(9)$$

$$\begin{split} OC_{WT_i} &= C_{OWT_i} (P_{WTs_i} - P_{WTa_i}) = \\ &= C_{OWT_i} \int_{0}^{P_{WTs_i}} (P_{WTs_i} - P_{WT_i}) f_{WT} (P_{WT_i}) dP_{WT_i}, \end{split} \tag{10}$$

where UC_{WT_i} , OC_{WT_i} are the underestimation and overestimation costs; C_{UWT_i} , C_{OWT_i} are the uncertainty cost coefficients; P_{WTs_i} , P_{WTa_i} , P_{WTr_i} are the scheduled, available and rated powers of the i^{th} wind unit.

For PV units, the uncertainty cost models are formulated as follows [12, 34]:

$$UC_{PV_{i}} = C_{UPV_{i}}(P_{PVa_{i}} - P_{PVS_{i}}) =$$

$$= C_{UPV_{i}} f_{PV}(P_{PVa_{i}} > P_{PVS_{i}}) [E(P_{PVa_{i}} > P_{PVS_{i}}) - P_{PVS_{i}}];$$
(11)

$$OC_{PV_i} = C_{OPV_i}(P_{PVS_i} - P_{PVa_i}) =$$

$$= C_{OPV_i} f_{PV}(P_{PVa_i} < P_{PVS_i}) [P_{PVS_i} - E(P_{PVa_i} > P_{PVS_i})],$$
(12)

where UC_{PV_i} , OC_{PV_i} are the underestimation and overestimation cost values, C_{UPV_i} , C_{OPV_i} are the uncertainty cost coefficients; P_{PVs_i} , P_{PVa_i} are the planned and available powers of the i^{th} PV unit.

Total cost function. The first objective F_1 aims to reduce the total cost, which includes the fuel cost of thermal units with VPE, as well as the costs associated with PV and WT units. The function F_1 is expressed as [35]:

$$F_{1} = \sum_{i=1}^{NTh} a_{i} + b_{i} P_{Th_{i}} + c_{i} P_{Th_{i}}^{2} + \left| d_{i} \sin(e_{i} (P_{Th_{i}}^{\min} - P_{Th_{i}})) \right| + \sum_{i=1}^{NWT} DC_{WT_{i}} + UC_{WT_{i}} + OC_{WT_{i}} + \sum_{i=1}^{NPV} DC_{PV_{i}} + UC_{PV_{i}} + OC_{PV_{i}}.$$
(13)

When the VPE is neglected, the objective function simplifies to:

$$F_{1} = \sum_{i=1}^{NTh} a_{i} + b_{i} P_{Th_{i}} + c_{i} P_{Th_{i}}^{2} + \sum_{i=1}^{NWT} DC_{WT_{i}} + UC_{WT_{i}} + OC_{WT_{i}} + \sum_{i=1}^{NPV} DC_{PV_{i}} + UC_{PV_{i}} + OC_{PV_{i}}.$$

$$(14)$$

Active power losses function. The second objective function F_2 aims to reduce the total active power losses, as formulated below [23, 36, 37]:

$$F_2 = \sum_{i=1}^{NTh} G_{ij}(n)(V_i^2 + V_j^2 - 2V_I V_J \cos \delta_{ij}), \qquad (15)$$

where $G_{ij}(n)$ is the conductance of the n^{th} branch; δ_{ij} is the voltage angle difference between buses i and j.

Voltage deviation function. The third objective function F_3 aims to reduce the voltage deviation and is expressed as follows [29, 38, 39]:

$$F_3 = \sum_{i=1}^{NPQ} |V_i - 1|.$$
 (16)

Multi-objective function. The fourth objective function F_4 originates from a multi-objective optimization problem that simultaneously considers total cost, active power losses and voltage deviation. These criteria are aggregated into a single scalar function using predefined weighting factors. It is described as follows:

$$F_4 = F_1 + \omega_1 F_2 + \omega_2 F_3, \tag{17}$$

where the total cost component is assigned a fixed weight of 1; ω_1 =100 and ω_2 =40 are the weighting factors for active power losses and voltage deviation. These values were chosen to ensure a balanced contribution of all objectives in the scalarized function. The weighting factors used in this study are the same as those adopted in previous works where a multi-objective function is constructed by combining single objectives such as cost, loss and voltage deviation [32].

Equality constraints. The solution to the OPF problem must satisfy the equality constraints defined as follows [40, 41]:

$$P_{G_i} = P_{D_i} + V_i \sum_{j=1}^{NB} V_j (G_{ij} \cos \delta_{ij} - B_{ij} \sin \delta_{ij}); \quad (18)$$

$$Q_{G_i} = Q_{D_i} + V_i \sum_{i=1}^{NB} V_j (G_{ij} \sin \delta_{ij} - B_{ij} \cos \delta_{ij}), \quad (19)$$

where P_{G_i} , Q_{G_i} are the real and reactive powers of the i^{th} generator, including thermal, WT and PV units; P_{D_i} , Q_{D_i} are the real and reactive loads.

Inequality constraint. Operational limits on power output and voltage levels for all generators are defined as constraints:

$$P_{Th_i}^{\min} \le P_{Th_i} \le P_{Th_i}^{\max}, \quad i = 1,...., NTh ;$$
 (20)

$$P_{WT_i}^{\min} \le P_{WT_i} \le P_{WT_i}^{\max}, \quad i = 1,, NWT;$$
 (21)

$$P_{PV_i}^{\min} \le P_{PV_i} \le P_{PV_i}^{\max}, \quad i = 1,...,NPV ;$$
 (22)

$$Q_{Th_i}^{\min} \le Q_{Th_i} \le Q_{Th_i}^{\max}, i = 1, ..., NTh;$$
 (23)

$$Q_{WT_i}^{\min} \le Q_{WT_i} \le Q_{WT_i}^{\max}, \quad i = 1, ..., NWT;$$
 (24)

$$Q_{PV_i}^{\min} \le Q_{PV_i} \le Q_{PV_i}^{\max}, \quad i = 1,...., NPV;$$
 (25)

$$V_{G_i}^{\min} \le V_{G_i} \le V_{G_i}^{\max}, \quad i = 1, ..., NG.$$
 (26)

The voltage at the PQ bus must remain within the specified limits:

$$V_{L_i}^{\min} \le V_{L_i} \le V_{L_i}^{\max}, \quad i = 1, ..., NPQ.$$
 (27)

The apparent power flow in each network branch must not exceed its allowable limits.

$$S_{L_i} \le S_{L_i}^{\text{max}}, \quad i = 1,, NS_L .$$
 (28)

Mathematical modeling of WT power uncertainty. The power of a WT is affected by wind speed variability and is represented by the Weibull PDF, as expressed in the following equation [34, 42]:

$$f_{v}(v) = \left(\frac{k}{c}\right) \cdot \left(\frac{v}{c}\right)^{k-1} e^{-\left(\frac{v}{c}\right)^{k}}; \tag{29}$$

where c is the scale parameter; k is the shape parameter.

The power supplied by a WT system is modeled as follows [34, 39]:

$$P_{WT}(v) = \begin{cases} 0; & \text{if } v_{out} < v; \ v_{in} < v; \\ P_{WTr} \left(\frac{v - v_{in}}{v_r - v_{in}} \right); & \text{if } v_r \le v \le v_{out}; \\ P_{WTr}; & \text{if } v_{in} \le v \le v_r, \end{cases}$$
(30)

where v_r , v_{out} , v_{in} are the rated, cut-out and cut-in wind speeds, which are equal to 16, 25 and 3 m/s.

Mathematical modeling of PV power uncertainty. The uncertainty in solar irradiance is modeled using a lognormal PDF, as defined in [34]:

$$f_{G_{PV}}(G_{PV}) = \frac{1}{G_{PV}\sigma\sqrt{2\pi}} \exp\left[-\frac{(\ln(G_{PV}) - \mu)^2}{2\sigma^2}\right] e^{\left(-\frac{v}{c}\right)^k}, (31)$$

where σ , μ are the standard deviations and mean values.

The power supplied by the PV system can be determined using the following equation [34, 43]:

$$P_{PV}(G_{PV}) = \begin{cases} P_{PVr} \left(\frac{G_{PV}^2}{G_{std} R_C} \right); & \text{if } 0 < G_{PV} \le R_C; \\ P_{PVr} \left(\frac{G_{PV}}{G_{std}} \right); & \text{if } G_{PV} \ge R_C, \end{cases}$$
(32)

where P_{PVr} is the rated power; R_c is the irradiance constant (set to 120 W/m²); G_{std} is the standard solar irradiance.

Blood-sucking leech optimizer is a recently introduced swarm intelligence algorithm proposed in [44]. This approach draws inspiration from the feeding mechanisms of blood-sucking leeches, particularly those observed in rice farming environments, where they attach to and feed on the blood of diverse hosts, including humans. The algorithm mimics the leeches' ability to locate prey using sensory receptors that detect stimuli like water waves. The behavioral dynamics of leeches are mathematically modeled by classifying them into 2 distinct categories. The first category, referred to as directional leeches, accurately processes the stimuli emitted by their prey, allowing them to advance incrementally toward the target with each iteration. In contrast, the second category, termed directionless leeches, misinterprets these signals and consequently moves away from the prey.

Initialization phase. The population of bloodsucking leeches is initialized randomly, as described in the following equation:

$$X = \operatorname{rand}(1, D)(ub - lb) + lb, \qquad (33)$$

where X is the position of all leeches; rand is the random number in the interval [0, 1]; D is the dimension of the optimization problem; ub, lb are the upper and lower bounds.

Exploration approach of directional leeches. During the exploration phase, the N_1 directional leeches move toward their prey at an angle α determined by their response to a circular wave stimulus. As these leeches approach the prey, the length L of the green arc, illustrated in Fig. 1 [44], gradually decreases. The number N_1 is calculated using the following equation:

$$N_1 = floor \left(N \left(m + (1 - m) \left(\frac{t}{T} \right)^2 \right) \right), \tag{34}$$

where t, T are the current and maximum iterations;

N is the population size. The MATLAB function *floor* is employed to round each element to the nearest integer that is less than or equal to the original value m, which is set to 0.8, serves as the ratio parameter.

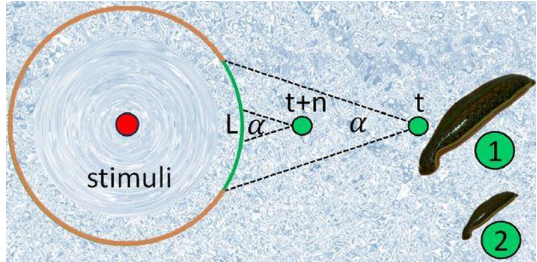


Fig. 1. Feeding mechanism of blood-sucking leeches [44]

The equations governing the exploration phase are:

$$x_{(i,j)}^{t+1} = \begin{cases} x_{(i,j)}^{t} + C \cdot x_{(i,j)}^{t} - L_{1}, & \text{if } r < a \text{ and } \left| x_{prey(j)} \right| > \left| x_{(i,j)}^{t} \right|; \\ x_{(i,j)}^{t} + C \cdot x_{(i,j)}^{t} + L_{1}, & \text{if } r < a \text{ and } \left| x_{prey(j)} \right| < \left| x_{(i,j)}^{t} \right|; \\ x_{(i,j)}^{t} + C \cdot x_{(i,j)}^{t} - L_{2}, & \text{if } r > a \text{ and } \left| x_{prey(j)} \right| > \left| x_{(i,j)}^{t} \right|; \\ x_{(i,j)}^{t} + C \cdot x_{(i,j)}^{t} + L_{2}, & \text{if } r > a \text{ and } \left| x_{prey(j)} \right| < \left| x_{(i,j)}^{t} \right|, \end{cases}$$

where a is the parameter of the BSLO method, assigned a value of 0.97. The term C represents the disturbance coefficient, which is defined as follows:

$$C = b \cdot \left(1 - \frac{t}{T}\right) \cdot 0.5 \cdot levy ; \tag{36}$$

$$levy = 0.01 \cdot \frac{\mu \cdot \sigma}{\left|\omega^{1/\beta}\right|}; \tag{37}$$

$$\sigma = \left(\frac{\Gamma(1+\beta) \cdot \sin(\pi\beta/2)}{\Gamma((1+\beta)/2) \cdot \beta \cdot 2^{(\beta-1)/2}}\right)^{1/\beta}; \quad (38)$$

$$\beta = -0.5 \cdot (t/T)^6 + (t/T)^4 + 1.5, \qquad (39)$$

where levy is the Levy flight distribution function; b, which is set to 0.001, is the parameter of the BSLO algorithm; μ , ω are the random numbers uniformly distributed within the interval [0, 1].

The lengths L_1 and L_2 are expressed as follows:

$$L_{1} = r_{1} \cdot \left| x_{prey(j)} - x_{(i,j)}^{t} \right| \cdot PD \cdot (1 - k_{1}/N); \tag{40}$$

$$L_2 = \left| x_{prey(j)} - x_{(i,k)}^t \right| \cdot PD \cdot \left(1 - r_1^2 \cdot \frac{k_1}{N} \right), \tag{41}$$

where k_1 is the random integer in the range [1, floor(N·(1 + t/T))]; k is the random integer in [1, m], while PD is the perceived distance. This parameter reflects the distance estimated by directional leeches from their prey and is calculated as:

$$PD = s \cdot r_2 \cdot (1 - t/T). \tag{42}$$

The value of *s* is given by the following expression:
$$s = \begin{cases} 8 - \left(-\left(t/T\right)^2 + 1\right) & \text{if } r < 0.5; \\ 8 - 7 \cdot \left(-\left(t/T\right)^2 + 1\right) & \text{else.} \end{cases}$$
(43)

Exploitation method Throughout this phase, the directional leeches progressively move closer to their prey, eventually reaching zones characterized by heightened stimulus intensity. The updated positions of these leeches are determined using the equations provided below:

$$x_{(i,j)}^{t+1} = \begin{cases} x_{(i,j)}^{t} + C \cdot x_{(i,j)}^{t} - L_{3}, & \text{if } r < a \text{ and } \left| x_{prey(j)} \right| > \left| x_{(i,j)}^{t} \right|; \\ x_{(i,j)}^{t} + C \cdot x_{(i,j)}^{t} + L_{3}, & \text{if } r < a \text{ and } \left| x_{prey(j)} \right| < \left| x_{(i,j)}^{t} \right|; \\ x_{(i,j)}^{t} + C \cdot x_{(i,j)}^{t} - L_{4}, & \text{if } r > a \text{ and } \left| x_{prey(j)} \right| > \left| x_{(i,j)}^{t} \right|; \\ x_{(i,j)}^{t} + C \cdot x_{(i,j)}^{t} + L_{4}, & \text{if } r > a \text{ and } \left| x_{prey(j)} \right| < \left| x_{(i,j)}^{t} \right|. \end{cases}$$

The value of b is set to 0.001 when (t<0.1T), and to 0.00001 in all other cases. This ensures that the distribution coefficient decreases progressively over successive iterations, allowing the BSLO algorithm to converge toward an optimal solution. The arc lengths L_3 and L_4 are defined as follows:

$$L_3 = \left| x_{prey(j)} - x_{(i,j)}^t \right| \cdot PD \cdot \left(1 - r_3^2 \cdot \frac{k_1}{N} \right); \quad (45)$$

$$L_4 = \left| x_{prey(j)} - x_{(i,k)}^t \right| \cdot PD \cdot \left(1 - r_3^2 \cdot \frac{k_1}{N} \right), \quad (46)$$

where the variables r, r_1 , r_2 and r_3 are the random numbers within the range [-1, 1].

Strategies transitioning between exploration and exploitation phases. The perceived distance PD acts as a critical decision-making parameter for directional leeches, facilitating their transition between the exploration and exploitation phases. $|PD| \ge 1$, a significant portion of the leeches are located at a distance from the prey, indicating that the BSLO algorithm is operating in the exploration phase. On the other hand, |PD| < 1, the leeches converge toward the prey, showing that the algorithm has entered the exploitation phase.

Search way of directionless leeches. The N_2 directionless leeches, calculated as $N_2 = N - N_1$, incorrectly respond to stimuli and move away from the target. Over successive iterations, their population size steadily diminishes, and their updated positions are determined as:

$$s = \begin{cases} \frac{t}{T} \cdot \left| x_{prey(j)} - x_{(i,j)}^t \right| \cdot 0.5 \cdot levy \cdot x_{(i,j)}^t, & \text{if } r < 0; \\ \frac{t}{T} \cdot \left| x_{prey(j)} - x_{(i,j)}^t \right| \cdot 0.5 \cdot levy \cdot x_{prey(j)}^t, & \text{else.} \end{cases}$$
(47)

Re-tracking approach. Following multiple iterations t_1 and after undergoing various phases of exploitation and exploration, certain leeches successfully located their prey (humans) and fed on their blood. Subsequently, the humans removed these leeches by returning them to the rice field. The updated positions of these leeches are mathematically expressed as follows:

$$X_i = \text{rand}(1, D) \cdot (ub - lb) + lb;$$

if $t > t_1$ and $F(X_i^t) = F(X_{prey}^{t-t_2}).$ (48)

The parameters t_1 and t_2 are assigned a value of 20. This approach ensures that the BSLO algorithm avoids becoming stuck in local optima. Figure 2 shows the flowchart of BSLO.

Simulations results. In this study, the performance and efficiency of the proposed BSLO algorithm were evaluated for solving the OPF problem in power systems integrating PV and WT systems. The tests were conducted on an IEEE 30-bus network, as described in [45], which includes 3 thermal generators at buses 1, 2, 8, one PV unit at bus 13, and 2 WT units at buses 5, 11. Additionally, the cost

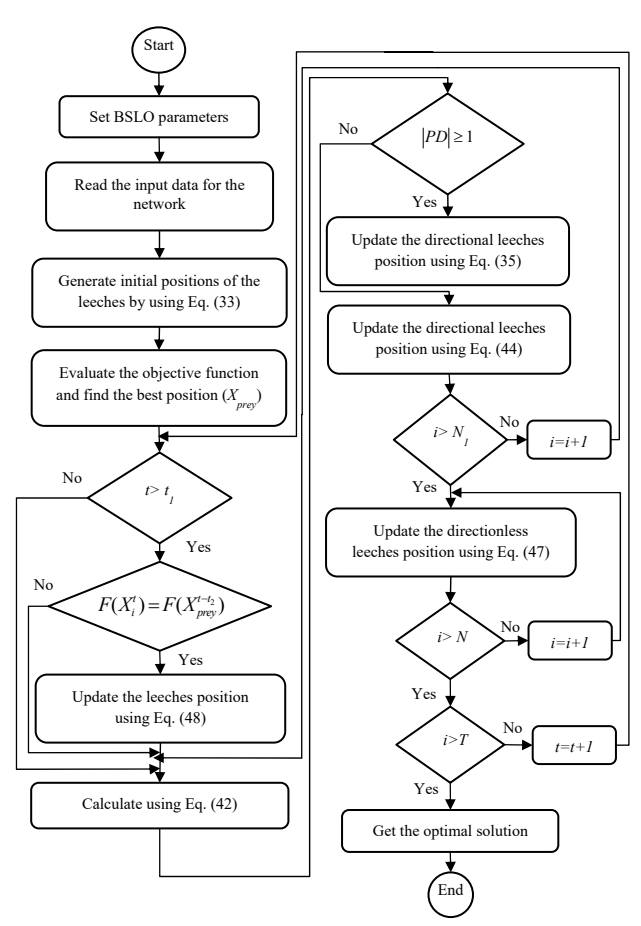


Fig. 2. BSLO flowchart

coefficients of the thermal generators, PV and WT units are detailed in [12, 29]. The second power system analyzed was the SEAN [46], consisting of 12 buses, 2 thermal generators, and 13 branches (including 2 transformers), with a total power demand of 297.5 MW and 39 MVAr. To assess the impact of renewable energy integration in this real network, a PV unit was incorporated at bus 8. Table 1 summarizes the main characteristics of the studied networks.

Table 1 Characteristics of the studied power systems

Item	IEEE 3	0-bus network	SEA	AN system
Item	Quantity	Details	Quantity	Details
Branches	41	[29]	13	[46]
Buses	30	[29]	12	[46]
Thermal units	3	buses: 1, 2, 8	2	buses: 1, 2
PV units	1	bus: 13	1	bus: 8
WT units	2	buses: 5, 11	_	_
Slack bus	1	bus: 1	1	bus: 1
Control variables	11	Real power at the PV buses and the voltage at the generator buses	5	Real power at the PV buses and the voltage at the generator buses
Rated power loads	_	283.4 MW, 126.2 MVAr	_	297.5 MW, 39 MVAr
PQ bus	24	[0.95-1.05] p.u.	8	[0.9–1.1] p.u.

Power flow analysis was performed using the MATPOWER [45]. The proposed BSLO algorithm was compared with PSO [47] and GWO [48]. To ensure a robust and consistent evaluation, 20 independent trial runs were conducted for all test cases. The population size (*N*=50) and the maximum number of iterations (*T*=300) were kept constant across all 3 optimization methods: BSLO, GWO and PSO.

The uncertainties in the power generated by the PV and WT units were considered in our study. The Monte Carlo simulation method was employed to generate 8000 values for both irradiation and wind speed. Tables 2, 3 present the cost coefficients of the thermal generators and the PV unit for the SEAN system.

Cost coefficients of thermal units for the SEAN system

Gen	Bus	a	b	c	
1	1	0	2.5	0.017	
2	2	0	2.5	0.017	

Table 3

Cost coefficients of PV units for the SEAN system

			2
Bus	C_{DPV}	OC_{PV}	UC_{PV}
8	1.6	3	1.5

Table 4 presents the Weibull PDF parameters of the WT units for the IEEE 30-bus network, while Table 5 reports the lognormal PDF parameters of the PV units for the IEEE 30-bus and SEAN systems.

Table 4

Weibull PDF parameters of WT units

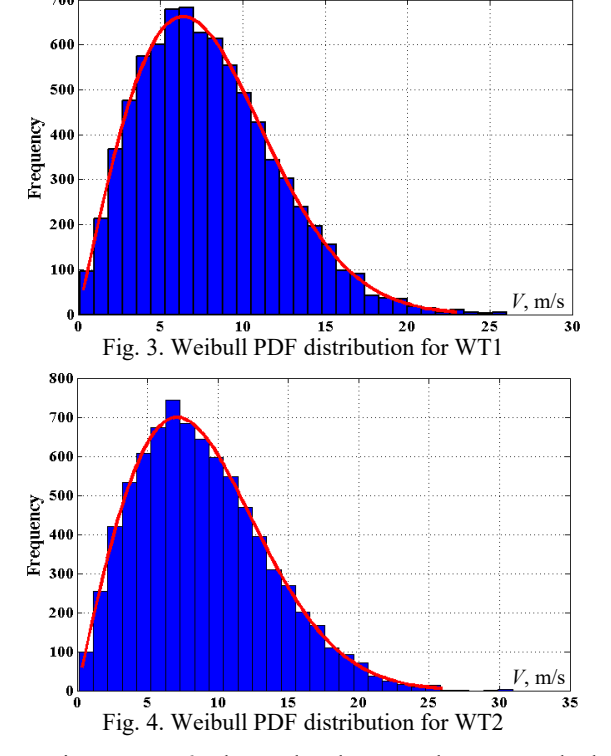
	P				
	IEEE 30-bus network				
Wind	No. of	Rated power Weibull PDF			
farm	turbines	P_{WTr} , MW	parameters		
WT1	25	75	c = 9, k = 2		
WT2	20	60	c = 10, k = 2		

Table 5

Lognormal PDF parameters of the PV units

Network	Rated power P_{PVr} , MW	Lognormal PDF parameters
IEEE30-bus	50 (bus 13)	$\mu = 6, \sigma = 0.6$
SEAN system	100 (bus 8)	$\mu = 6, \sigma = 0.6$

Figures 3, 4 show the Weibull fitting and the wind speed frequency distribution for the wind power plants that replaced thermal generators at buses 5 (WT1) and 11 (WT2) in the IEEE 30-bus network. These results were obtained after performing 8000 Monte Carlo simulations.



Figures 5, 6 show the lognormal PDF and the irradiance frequency distribution obtained from Monte Carlo

simulations with 8000 iterations. These results correspond to the PV unit installed at bus 13, which replaces the thermal generator in the IEEE 30-bus system, and the additional PV unit integrated at bus 8 of the SEAN system.

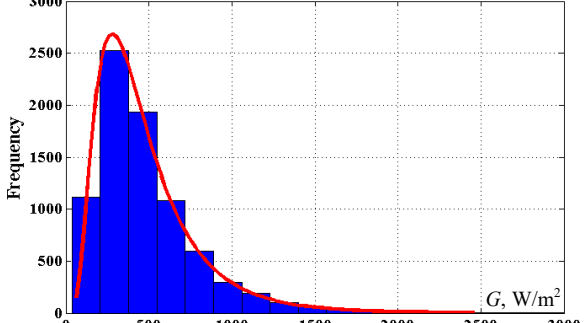
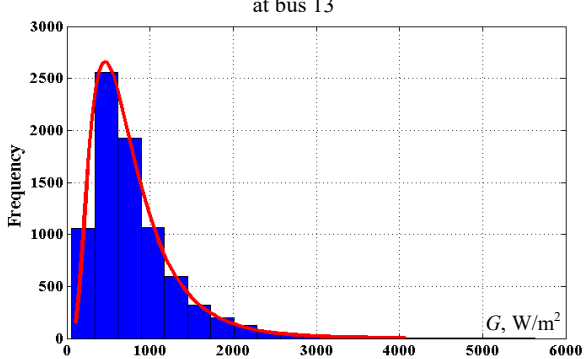


Fig. 5. Lognormal PDF for the solar PV in the IEEE 30-bus system at bus 13



0 1000 2000 3000 4000 5000 6000 Fig. 6. Lognormal PDF for the solar PV in the SEAN system at bus 8

Figures 7, 8 illustrate the stochastic output power of the PV units in each of the power systems under study. This distribution is used to calculate the overestimation and underestimation costs of the solar PV units based on their scheduled power output.

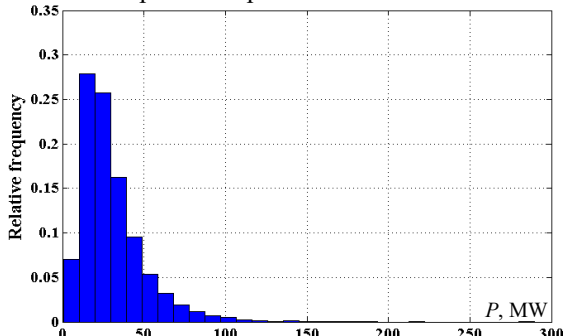


Fig. 7. Real power distribution of the PV unit in the IEEE 30-bus network at bus 13

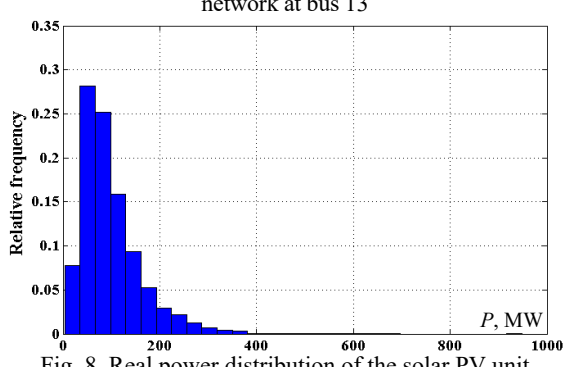


Fig. 8. Real power distribution of the solar PV unit in the SEAN system at bus 8

Test results of the IEEE30-bus system. Total cost minimizing. The first case study aims to reduce the total

cost function (F_1) with VPE as signaled in (13), and includes wind, solar and conventional power generation. The direct costs of wind and solar energy are calculated using (7), (8). Additionally, the underestimation and overestimation costs for wind and solar energy are determined using (9), (11) and (10), (12), respectively.

Table 6 presents the optimal results for the decision variables, reactive power of generators, total generation cost, power losses and total voltage deviation obtained using the BSLO, GWO and PSO algorithms. The table also includes the mean, standard deviation (Std) and worst value of the total generation cost. Additionally, the minimum and maximum values of the real and reactive power of the generators, as well as the voltage amplitude, are provided in Table 6 and are identical across all scenarios considered for the IEEE 30-bus system.

Table 6 Simulation results for total cost reduction

Simulation results for total cost reduction					
Item	min	max	PSO	GWO	BSLO
$P_{\mathrm{Th1}},\mathrm{MW}$	50	140	76.7121	71.6108	64.2158
P_{Th2} , MW	20	80	35.8849	37.87	38.7185
$P_{\mathrm{Th3}},\mathrm{MW}$	10	35	24.6507	33.1131	35
P_{WTs1} , MW	0	75	68.5834	66.3579	68.7485
P_{WTs2} , MW	0	60	42.4412	41.7435	44.9998
$P_{\text{PVs1}}, \text{MW}$	0	50	38.3328	35.6942	34.442
V_1 , p.u.	0.95	1.1	1.0239	1.0277	1.0268
V_2 , p.u.	0.95	1.1	1.0154	1.0199	1.0198
V_5 , p.u.	0.95	1.1	0.9973	1.0037	1.0076
V_8 , p.u.	0.95	1.1	0.9982	1.0062	1.0077
V ₁₁ , p.u.	0.95	1.1	1.0082	1.0358	1.0234
V ₁₃ , p.u.	0.95	1.1	1.0307	1.0167	1.0166
Q_{Th1} , MVAr	-20	150	1.2899	0.7484	0.8544
Q_{Th2} , MVAr	-20	60	20.6716	18.7892	16.13
Q_{Th3} , MVAr	-15	40	38.7294	39.4339	40
Q_{WTs1} , MVAr	-30	35	21.3278	22.7235	25.4271
Q_{WTs2} , MVAr	-10	30	1.044	8.1244	7.0903
Q_{PVs1} , MVAr	-20	25	4.8243	-3.2843	-3.2947
Total cost, \$/h, best	_	_	785.4689	785.8805	781.22
P_{Loss} , MW	_	_	5.9874	6.4032	5.798
VD, p.u.	_	_	0.5054	0.4957	0.7169
Mean	_	_	796.4208	806.673	781.5035
Worst	_	_	816.4433	837.7390	782.1341
Std	_	_	7.2581	16.9356	0.2328

The results show that the BSLO algorithm achieves the lowest total generation cost among the compared methods, with a value of 781.22 \$/h, compared to 785.4689 \$/h for PSO and 785.8805 \$/h for GWO. Moreover, the standard deviation for BSLO is notably low (0.2328) compared to PSO (7.2581) and GWO (16.9356), indicating that the results obtained by BSLO exhibit minimal dispersion across the 20 simulations conducted. This demonstrates the algorithm's stable convergence and enhanced reliability. Furthermore, as shown in Fig. 9, the BSLO algorithm converges to the optimal solution in less iteration, highlighting its efficiency and fast convergence behavior.

Total active power losses minimizing. This case study focuses on minimizing total active transmission losses in the IEEE 30-bus system using the BSLO, GWO and PSO algorithms. As shown in Table 7, the BSLO algorithm achieves the lowest power losses with a value of 2.0369 MW, compared to 2.5869 MW for PSO and 2.7671 MW for GWO, and demonstrates strong performance in terms of both the mean and standard deviation.

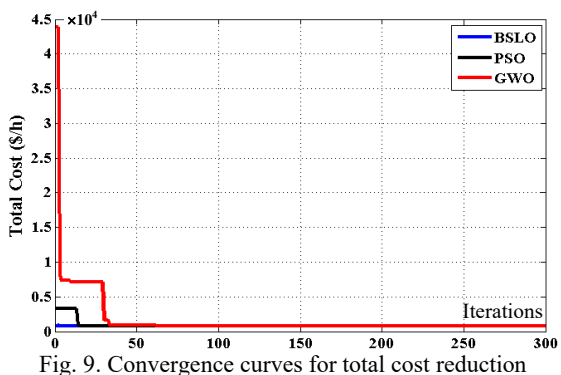


Table 7
Simulation results for total active power losses reduction

Item	PSO	GWO	BSLO
$P_{\mathrm{Th1}},\mathrm{MW}$	56.7554	76.0841	50
P_{Th2} , MW	43.7425	33.4933	29.4619
P_{Th3} , MW	32.1789	28.1790	35
P_{WTs1} , MW	71.2795	74.9682	75
P_{WTs2} , MW	55.484	49.0042	59.9997
$P_{\text{PVs1}}, \text{MW}$	26.5466	24.4383	35.9753
V_1 , p.u.	1.0359	1.0398	1.0399
V_2 , p.u.	1.0264	1.0311	1.0339
V_5 , p.u.	1.016	1.02	1.0232
V_8 , p.u.	1.0102	1.0212	1.0287
<i>V</i> ₁₁ , p.u.	1.0604	1.0726	1.0684
V_{13} , p.u.	0.989	1.0485	1.048
$Q_{Th1}, MVAr$	10.4175	-0.2533	-0.3096
Q_{Th2} , MVAr	12.1398	9.9067	11.2841
Q_{Th3} , MVAr	35.8329	37.2458	39.8119
Q_{WTs1} , MVAr	27.4807	22.2697	21.3692
Q_{WTs2} , MVAr	17.319	14.1711	12.7728
Q_{PVs1} , MVAr	-14.5685	0.7956	-0.6847
Total cost, \$/h	874.3381	864.1246	879.3848
P_{Loss} , MW, best	2.5869	2.7671	2.0369
VD, p.u.	0.2398	0.6	0.6595
Mean	3.1307	3.8534	2.0654
Worst	4.4579	6.2984	2.1569
Std	0.4426	0.8314	0.0294

Figure 10 presents the convergence curves corresponding to the best results obtained with PSO, GWO and BSLO, highlighting the evolution of minimal active power line losses. It is evident that the objective function value decreases rapidly and stabilizes in fewer than 20 iterations when using the BSLO algorithm, confirming its fast convergence capability.

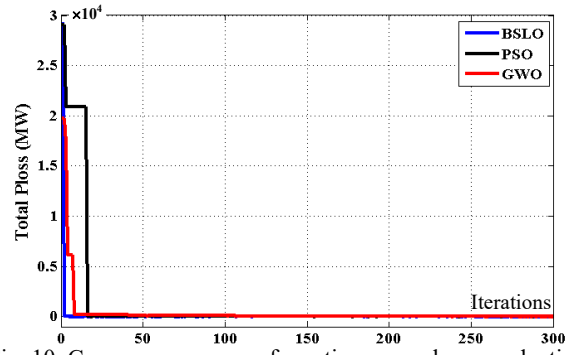


Fig. 10. Convergence curves for active power losses reduction

Load voltage deviation minimizing. This case interests on controlling the voltage magnitudes of load buses by minimizing their deviations from the reference value ($V_{ref} = 1$ p.u.), as defined in (16). Table 8 summarizes

the simulation results voltage deviation reduction, highlighting that the BSLO algorithm achieves the lowest value (0.1913 p.u.), compared to 0.208 p.u. for PSO and 0.2014 p.u. for GWO. The convergence curves of the evaluated methods are illustrated in Fig. 11. Furthermore, the BSLO algorithm converges to the global solution with a smaller number of iterations.

Table 8 Simulation results for voltage deviation reduction

Similaration 10	Simulation results for voltage deviation reduction						
Item	PSO	GWO	BSLO				
$P_{\mathrm{Th1}},\mathrm{MW}$	88.2113	119.1021	55.2959				
P_{Th2} , MW	45.6265	29.9804	80				
P_{Th3} , MW	27.2619	28.7075	35				
P_{WTs1} , MW	70.0671	69.8552	74.4709				
P_{WTs2} , MW	36.6761	25.5604	41.9836				
$P_{\mathrm{PVs1}},\mathrm{MW}$	19.3226	15.0478	0				
V_1 , p.u.	1.0308	1.0325	1.0256				
V_2 , p.u.	1.0301	1.0303	1.0322				
V_5 , p.u.	1.0098	1.0163	1.0165				
V_8 , p.u.	1.0048	1.0052	1.0067				
V ₁₁ , p.u.	1.0166	1.0123	1.0023				
V_{13} , p.u.	1.0079	1.0157	1.0181				
Q_{Th1} , MVAr	-14.4918	-19.4105	-19.9972				
Q_{Th2} , MVAr	44.6989	45.4807	45.9197				
Q_{Th3} , MVAr	39.2687	39.3375	40				
Q_{WTs1} , MVAr	22.4846	28.859	26.2698				
Q_{WTs2} , MVAr	2.058	-0.5398	-2.6237				
Q_{PVs1} , MVAr	-5.1563	-2.5165	0.374				
Total cost, \$/h	862.069	849.3795	958.0732				
P_{Loss} , MW	3.7656	4.8534	3.3503				
VD, p.u., best	0.208	0.2014	0.1913				
Mean	0.2224	0.2113	0.1924				
Worst	0.2422	0.2245	0.1962				
Std	0.0083	0.0074	0.0011				

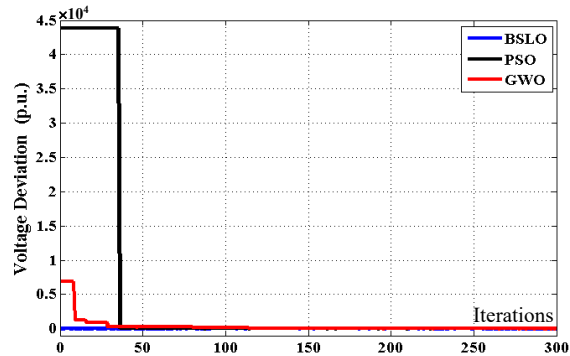


Fig. 11. Convergence curves for voltage deviation reduction

Multi-objective function minimizing. The objective is to minimize the multi-objective function defined in (17), which includes the total generation cost, active power losses and load voltage deviation. Table 9 presents the OPF solutions obtained using the BSLO, GWO and PSO algorithms. The BSLO algorithm demonstrates superior performance compared to the other methods. Moreover, the convergence curve of the objective function is illustrated in Fig. 12. The evolution of the multi-objective function using BSLO also shows the most favorable behavior among the evaluated algorithms.

The superiority of the BSLO algorithm is particularly evident in the multi-objective optimization case. Unlike PSO and GWO, which show significant variability between runs, with standard deviations of 19.5146 and 46.9889 and large gaps between worst and

best objective values (1064.8796 versus 993.1464 for PSO, and 1180.1231 versus 996.7087 for GWO, BSLO exhibits remarkable consistency. It achieves a worst-case value of 985.8281, a best-case value of 985.3818, and a very low standard deviation of 0.1058, confirming its robustness and reliability. In this case, using BSLO, the total active losses are 2.2949 MW, the voltage drop (*VD*) is 0.2252 p.u., and the generation cost is \$871.0642 \$/h.

Simulation results for multi-objective function minimization

Item	PSO	GWO	BSLO
$P_{\mathrm{Th1}},\mathrm{MW}$	60.258	76.0573	50
$P_{\mathrm{Th2}},\mathrm{MW}$	34.9418	34.4584	35.4247
$P_{\mathrm{Th3}},\mathrm{MW}$	24.6371	23.8389	35
P_{WTs1} , MW	74.0053	72.7683	73.722
P_{WTs2} , MW	51.2131	42.651	50.3174
$P_{\mathrm{PVs1}},\mathrm{MW}$	41.0924	36.6089	41.2308
V_1 , p.u.	1.037	1.0252	1.0208
V_2 , p.u.	1.0252	1.0196	1.0151
<i>V</i> ₅ , p.u.	1.0226	1.007	1.005
V_8 , p.u.	1.01	1.0052	1.0063
<i>V</i> ₁₁ , p.u.	1.0151	1.0522	1.0365
V_{13} , p.u.	1.025	1.0095	1.0184
Q_{Th1} , MVAr	12.8347	-5.4173	0.34
Q_{Th2} , MVAr	3.6808	21.8226	13.8981
Q_{Th3} , MVAr	36.645	39.1846	40
Q_{WTs1} , MVAr	34.107	24.016	24.6231
Q_{WTs2} , MVAr	1.0662	13.8226	9.4904
Q_{PVs1} , MVAr	-1.1077	-6.3064	-2.0071
Total cost, \$/h	862.5596	850.8861	871.0642
P_{Loss} , MW	2.648	3.0731	2.2949
VD, p.u.	0.2467	0.229	0.2252
Multi-objective function F_4 , best	993.1464	996.7087	985.3818
Mean	1021.5482	1043.9233	985.4953
Worst	1064.8796	1180.1231	985.8281
Std	19.5146	46.9889	0.1058

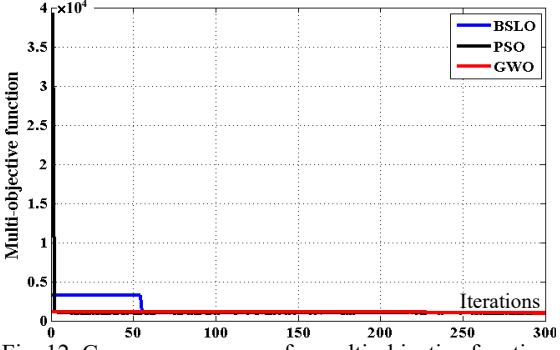
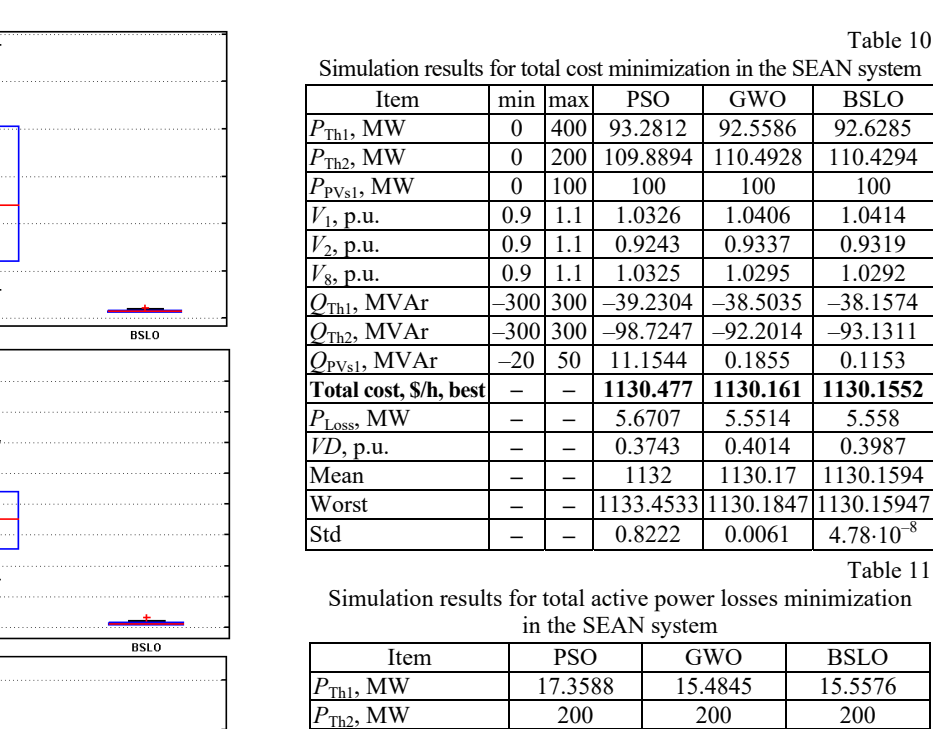


Fig. 12. Convergence curves for multi-objective function minimization

To assess the performance of the BSLO algorithm, the results of 20 independent runs conducted for each method are presented as boxplots in Fig. 13, offering a clear visual comparison of result dispersion, stability, and robustness. The analysis shows that BSLO achieves significantly lower dispersion than the other algorithms, indicating more stable convergence and greater reliability. BSLO consistently produces results that are less affected by variations in the initial decision variables. Note that each algorithm includes a population initialization phase, which is inherently random and can significantly influence the algorithm's ability to find the global optimum of the problem.



 $P_{\text{Th2}}, \overline{\text{MW}}$ $P_{\mathrm{PVs1}}, \mathrm{MW}$ 81.8412 83.7122 83.6391 V_1 , p.u. 0.9883 0.983 0.9822 0.9495 V_2 , p.u. 0.9422 0.9418 1.038 1.0321 1.0313 V_8 , p.u. 49.5131 48.2966 48.3258 $Q_{\text{Th1}}, M\text{VAr}$ $Q_{\text{Th2}}, \overline{\text{MVAr}}$ 75.7063 -75.2507 -74,4846 $Q_{\text{PVs1}}, \overline{\text{MVAr}}$ -0.6789 -0.8503 0.985 Total cost, \$/h 1446.8353 1445.6603 1445.6729 $P_{\text{Loss}}, \overline{\text{MW}}, \text{best}$ 1.6967 1.6967 1.7 VD, p.u. 0.3824 0.3284 0.3222 Mean 1.7129 1.6969 1.6967 Worst 1.697 1.69677 1.7643 0.0166 Std $6.8336 \cdot 10^{-1}$ 5.2117.10

Table 12

OPF simulation results for voltage deviation minimization in the SEAN system

Item	PSO	GWO	BSLO
$P_{\mathrm{Th1}},\mathrm{MW}$	198.3750	208.1016	212.7295
P_{Th2} , MW	74.3085	98.7613	43.0739
$P_{\mathrm{PVs1}},\mathrm{MW}$	51.4712	20.4118	72.4242
V_1 , p.u.	0.9838	0.9875	0.9898
V_2 , p.u.	0.9744	0.9749	0.9883
V_8 , p.u.	1.0015	1.0026	1.0011
Q_{Th1} , MVAr	-0.5315	6.333	9.6434
Q_{Th2} , MVAr	-26.5009	-23.7497	-13.5178
Q_{PVs1} , MVAr	8.8667	19.0264	2.8416
Total cost, \$/h	1610.6879	1820.7532	1642.4949
P_{Loss} , MW	26.6548	29.7748	30.7277
VD, p.u., best	0.01526	0.01469	0.01386
Mean	0.0202	0.0239	0.0141
Worst	0.03014	0.0398	0.01517
Std	0.004	0.0074	$2.9827 \cdot 10^{-4}$

Multi-objective function in SEAN system. The multiobjective function of the OPF problem simultaneously considers the generation cost of both thermal generators and solar PV units, the voltage profile and power losses (Fig. 17). Table 13 summarizes the values of the decision parameters, the reactive power outputs of all generators, the objective function values, and the statistical performance indicators obtained using the PSO, GWO, and BSLO algorithms.

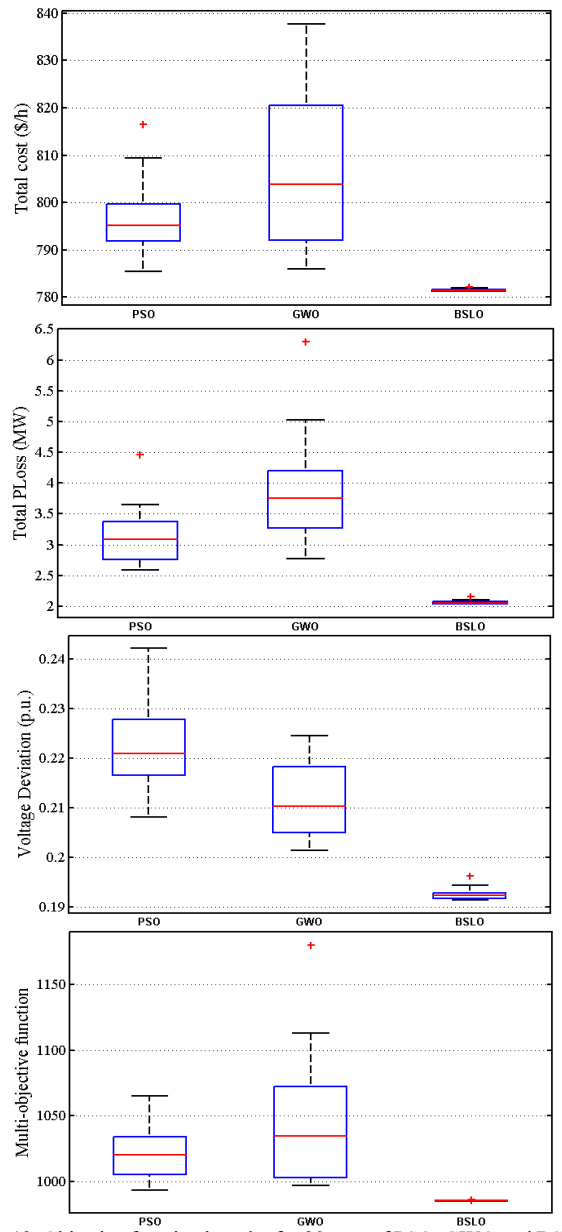
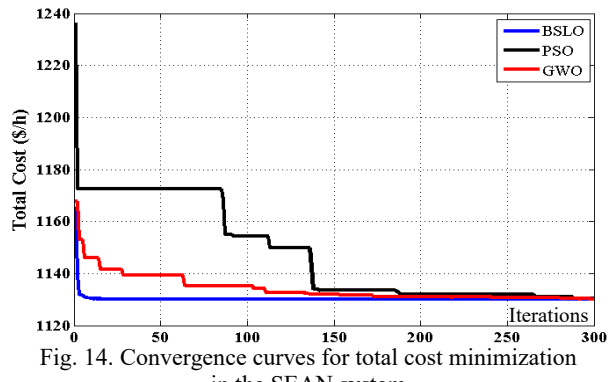


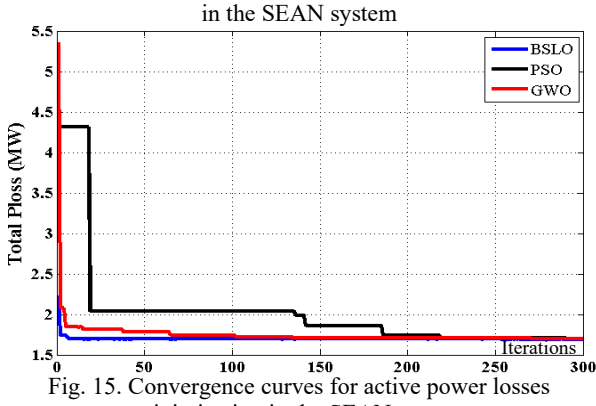
Fig. 13. Objective function boxplot for 20 runs of PSO, GWO and BSLO

Test results of the SEAN. Single objective function in SEAN system. In this section, the PSO, GWO and BSLO algorithms were applied to the real SEAN system to address 3 single objective functions: minimizing the total generation cost without VPE (case 1), minimizing total active power losses (case 2) and minimizing voltage deviation (case 3). The simulation results obtained using the different algorithms for the single objective optimization cases 1–3 are presented in Tables 10–12.

These results show that the BSLO method provides the best OPF solutions compared to the other methods. In case 1, which focuses on minimizing the total generation cost, the values obtained are 1130.477 \$/h, 1130.161 \$/h and 1130.1552 \$/h using the PSO, GWO and BSLO algorithms, respectively. In case 2, the BSLO algorithm achieves the lowest power losses at 1.6967 MW, and in case 3, it also provides the smallest voltage deviation at 0.01386 p.u. In all single objective function, the statistical performance indicators: best, mean, worst and standard deviation demonstrate that BSLO consistently outperforms both PSO and GWO. Also, the BSLO algorithm exhibits a faster convergence rate, as illustrated in Fig. 14–16.

In this case, the BSLO algorithm once again outperforms the other methods, achieving the lowest objective function value of 1333.8135.





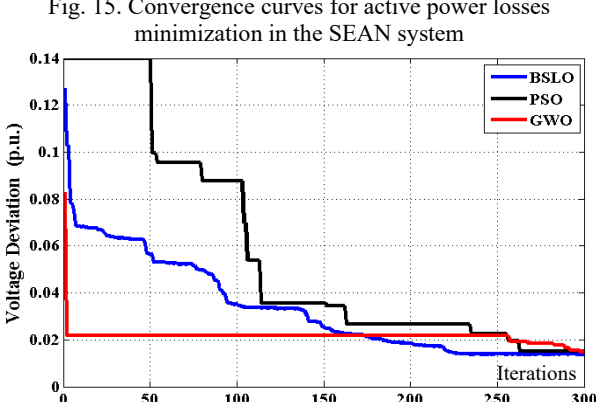


Fig. 16. Convergence curves for voltage deviation minimization in the SEAN system

Table 13 Simulation results for multi-objective function minimization in the SEAN system

Item	PSO	GWO	BSLO			
$P_{\mathrm{Th1}},\mathrm{MW}$	0.5917	57.2208	57.4852			
P_{Th2} , MW	141.4894	143.2943	143.0508			
$P_{\mathrm{PVs1}},\mathrm{MW}$	100	100	100			
V_1 , p.u.	0.9612	0.9668	0.9657			
V_2 , p.u.	0.92	0.919	0.9201			
V_8 , p.u.	1.001	1.0006	1.0001			
Q_{Th1} , MVAr	-46.6739	-45.8008	-45.9652			
Q_{Th2} , MVAr	-72.6615	-73.294	-72.2996			
Q_{PVs1} , MVAr	-1.6825	-2.5963	-3.4911			
Total cost, \$/h	1170.8346	1175.3552	1174.737			
P_{Loss} , MW	3.1595	3.01522	3.0360			
VD, p.u.	0.09741	0.1074	0.1056			
Multi-objective function F ₄ , best	1334.1308	1333.8270	1333.8135			
Mean	1341.4334	1333.8567	1333.8136			
Worst	1360.9850	1333.9529	1333.8137			
Std	7.3014	0.03114	6.0958×10 ⁻⁵			

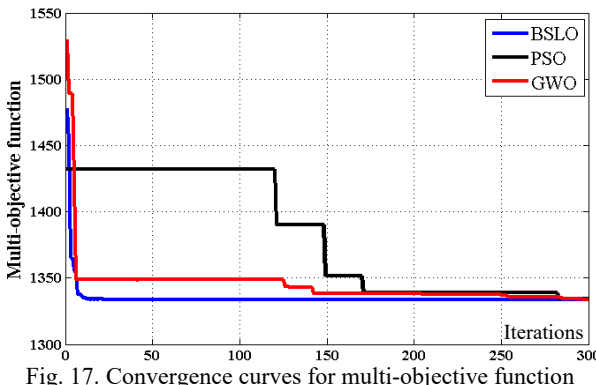


Fig. 17. Convergence curves for multi-objective function minimization in the SEAN system

In comparison to the IEEE-30 bus network, no significant difference in the best values is observed between the 3 algorithms for the various objective functions in the SEAN system. This is due to the fact that the number of decision variables is only 5 in the Algerian network, whereas it is 11 in the IEEE-30 bus network.

Conclusions. This paper presents a solution methodology for addressing the OPF problem in electrical grids integrating PV and WT generators. The inherent uncertainties of intermittent renewable energy sources are modeled using PDF and Monte Carlo simulations. To solve the OPF problem, BSLO algorithm was effectively employed, and its computational efficiency was compared against the PSO and GWO algorithms. Four distinct objective functions were considered:

- minimization of total generation costs from thermal and renewable sources;
 - reduction of active power losses;
 - voltage deviation minimization;
- a multi-objective function combining all 3 through a weighted sum.

The proposed approach was tested on the both the IEEE 30-bus test system, which includes stochastic wind and solar power units, and a real-world power system in the Southeast Algeria, incorporating the variability of PV generation. The results demonstrate that addressing the stochastic OPF problem significantly improves grid performances. Optimal integration of renewable energy sources leads to reduce the active power supplied by the thermal generators and minimizing overall generation costs. Moreover, the BSLO algorithm demonstrated superior convergence characteristics and solution quality compared to PSO and GWO algorithms across all case studies, achieving the most optimal solutions for the OPF problem. These findings highlight the effectiveness and robustness of the BSLO algorithm for solving complex stochastic OPF problems.

Conflict of interest. The authors declare that they have no conflicts of interest.

REFERENCES

- 1. Carpentier J. Optimal power flows. *International Journal of Electrical Power & Energy Systems*, 1979, vol. 1, no. 1, pp. 3-15. doi: https://doi.org/10.1016/0142-0615(79)90026-7.
- 2. Capitanescu F., Martinez Ramos J.L., Panciatici P., Kirschen D., Marano Marcolini A., Platbrood L., Wehenkel L. State-of-the-art, challenges, and future trends in security constrained optimal power flow. *Electric Power Systems*

- Research, 2011, vol. 81, no. 8, pp. 1731-1741. doi: https://doi.org/10.1016/j.epsr.2011.04.003.
- 3. Naderi E., Narimani H., Pourakbari-Kasmaei M., Cerna F.V., Marzband M., Lehtonen M. State-of-the-Art of Optimal Active and Reactive Power Flow: A Comprehensive Review from Various Standpoints. *Processes*, 2021, vol. 9, no. 8, art. no. 1319. doi: https://doi.org/10.3390/pr9081319.
- 4. Lai L.L., Ma J.T., Yokoyama R., Zhao M. Improved genetic algorithms for optimal power flow under both normal and contingent operation states. *International Journal of Electrical Power & Energy Systems*, 1997, vol. 19, no. 5, pp. 287-292. doi: https://doi.org/10.1016/S0142-0615(96)00051-8.
- **5.** Abido M.A. Optimal power flow using particle swarm optimization. *International Journal of Electrical Power & Energy Systems*, 2002, vol. 24, no. 7, pp. 563-571. doi: https://doi.org/10.1016/S0142-0615(01)00067-9.
- **6.** Bakirtzis A.G., Biskas P.N., Zoumas C.E., Petridis V. Optimal power flow by enhanced genetic algorithm. *IEEE Transactions on Power Systems*, 2002, vol. 17, no. 2, pp. 229-236. doi: https://doi.org/10.1109/TPWRS.2002.1007886.
- 7. Roa-Sepulveda C.A., Pavez-Lazo B.J. A solution to the optimal power flow using simulated annealing. *International Journal of Electrical Power & Energy Systems*, 2003, vol. 25, no. 1, pp. 47-57. doi: https://doi.org/10.1016/S0142-0615(02)00020-0.
- 8. Somasundaram P., Kuppusamy K., Kumudini Devi R.P. Evolutionary programming based security constrained optimal power flow. *Electric Power Systems Research*, 2004, vol. 72, no. 2, pp. 137-145. doi: https://doi.org/10.1016/j.epsr.2004.02.006.
- 9. Si Tayeb A., Larouci B., Rezzak D., Houam Y., Bouzeboudja H., Bouchakour A. Application of a new hybridization to solve economic dispatch problem on an Algerian power system without or with connection to a renewable energy. *Diagnostyka*, 2021, vol. 22, no. 3, pp. 101-112. doi: https://doi.org/10.29354/diag/142060.
- 10. Marzbani F., Abdelfatah A. Economic Dispatch Optimization Strategies and Problem Formulation: A Comprehensive Review. *Energies*, 2024, vol. 17, no. 3, art. no. 550. doi: https://doi.org/10.3390/en17030550.
- 11. Sulaiman M.H., Mustaffa Z. Optimal power flow incorporating stochastic wind and solar generation by metaheuristic optimizers. *Microsystem Technologies*, 2021, vol. 27, no. 9, pp. 3263-3277. doi: https://doi.org/10.1007/s00542-020-05046-7.
- **12.** Ghasemi M., Trojovský P., Trojovská E., Zare M. Gaussian bare-bones Levy circulatory system-based optimization for power flow in the presence of renewable units. *Engineering Science and Technology, an International Journal*, 2023, vol. 47, art. no. 101551. doi: https://doi.org/10.1016/j.jestch.2023.101551.
- 13. Naidji M., Boudour M. Stochastic multi-objective optimal reactive power dispatch considering load and renewable energy sources uncertainties: a case study of the Adrar isolated power system. *International Transactions on Electrical Energy Systems*, 2020, vol. 30, no. 6. doi: https://doi.org/10.1002/2050-7038.12374.
- 14. Kouadri R., Slimani L., Bouktir T., Musirin I. Optimal Power Flow Solution for Wind Integrated Power in presence of VSC-HVDC Using Ant Lion Optimization. *Indonesian Journal of Electrical Engineering and Computer Science*, 2018, vol. 12, no. 2, pp. 625-633. doi: https://doi.org/10.11591/ijeecs.v12.i2.pp625-633.
- 15. Wells D.W. Method for economic secure loading of a power system. *Proceedings of the Institution of Electrical Engineers*, 1968, vol. 115, no. 8, art. no. 1190. doi: https://doi.org/10.1049/piee.1968.0210.
- 16. Habibollahzadeh H., Luo G.-X., Semlyen A. Hydrothermal optimal power flow based on a combined linear and nonlinear programming methodology. *IEEE Transactions on Power Systems*, 1989, vol. 4, no. 2, pp. 530-537. doi: https://doi.org/10.1109/59.193826.

- 17. Ponnambalam K., Quintana V.H., Vannelli A. A fast algorithm for power system optimization problems using an interior point method. *IEEE Transactions on Power Systems*, 1992, vol. 7, no. 2, pp. 892-899. doi: https://doi.org/10.1109/59.141801.
- 18. Sun D., Ashley B., Brewer B., Hughes A., Tinney W. Optimal Power Flow By Newton Approach. *IEEE Transactions on Power Apparatus and Systems*, 1984, vol. PAS-103, no. 10, pp. 2864-2880. doi: https://doi.org/10.1109/TPAS.1984.318284. 19. Santos A., da Costa G.R.M. Optimal-power-flow solution by
- Newton's method applied to an augmented Lagrangian function. *IEE Proceedings: Generation, Transmission and Distribution*, 1995, vol. 142, no. 1, pp. 33-36. doi: https://doi.org/10.1049/ipgtd:19951586.
- 20. Nicholson H., Sterling M. Optimum Dispatch of Active and Reactive Generation by Quadratic Programming. *IEEE Transactions on Power Apparatus and Systems*, 1973, vol. PAS-92, no. 2, pp. 644-654. doi: https://doi.org/10.1109/TPAS.1973.293768.
- 21. Diab A.A.Z., Abdelhamid A.M., Sultan H.M. Comprehensive analysis of optimal power flow using recent metaheuristic algorithms. *Scientific Reports*, 2024, vol. 14, no. 1, art. no. 13422. doi: https://doi.org/10.1038/s41598-024-58565-y.
- 22. Surender Reddy S., Bijwe P.R. Efficiency improvements in meta-heuristic algorithms to solve the optimal power flow problem. *International Journal of Electrical Power & Energy Systems*, 2016, vol. 82, pp. 288-302. doi: https://doi.org/10.1016/j.ijepes.2016.03.028.
- 23. Nassef A.M., Abdelkareem M.A., Maghrabie H.M., Baroutaji A. Review of Metaheuristic Optimization Algorithms for Power Systems Problems. *Sustainability*, 2023, vol. 15, no. 12, art. no. 9434. doi: https://doi.org/10.3390/su15129434.
- 24. Abbas M., Alshehri M.A., Barnawi A.B. Potential Contribution of the Grey Wolf Optimization Algorithm in Reducing Active Power Losses in Electrical Power Systems. *Applied Sciences*, 2022, vol. 12, no. 12, art. no. 6177. doi: https://doi.org/10.3390/app12126177.
- 25. Tehzeeb-Ul-Hassan H., Tahir M.F., Mehmood K., Cheema K.M., Milyani A.H., Rasool Q. Optimization of power flow by using Hamiltonian technique. *Energy Reports*, 2020, vol. 6, pp. 2267-2275. doi: https://doi.org/10.1016/j.egyr.2020.08.017.
- **26.** Pradhan M., Roy P.K., Pal T. Grey wolf optimization applied to economic load dispatch problems. *International Journal of Electrical Power & Energy Systems*, 2016, vol. 83, pp. 325-334. doi: https://doi.org/10.1016/j.ijepes.2016.04.034.
- 27. Varadarajan M., Swarup K.S. Solving multi-objective optimal power flow using differential evolution. *IET Generation, Transmission & Distribution*, 2008, vol. 2, no. 5, pp. 720-730. doi: https://doi.org/10.1049/iet-gtd:20070457.
- 28. Alghamdi A.S., Zohdy M.A. Boosting cuckoo optimization algorithm via Gaussian mixture model for optimal power flow problem in a hybrid power system with solar and wind renewable energies. *Heliyon*, 2024, vol. 10, no. 11, art. no. e31755. doi: https://doi.org/10.1016/j.heliyon.2024.e31755.
- **29.** Biswas P.P., Suganthan P.N., Amaratunga G.A.J. Optimal power flow solutions incorporating stochastic wind and solar power. *Energy Conversion and Management*, 2017, vol. 148, pp. 1194-1207. doi: https://doi.org/10.1016/j.enconman.2017.06.071.
- *30.* Guvenc U., Duman S., Kahraman H.T., Aras S., Katı M. Fitness–Distance Balance based adaptive guided differential evolution algorithm for security-constrained optimal power flow problem incorporating renewable energy sources. *Applied Soft Computing*, 2021, vol. 108, art. no. 107421. doi: https://doi.org/10.1016/j.asoc.2021.107421.
- *31.* Meng A., Zeng C., Wang P., Chen D., Zhou T., Zheng X., Yin H. A high-performance crisscross search based grey wolf optimizer for solving optimal power flow problem. *Energy*, 2021, vol. 225, art. no. 120211. doi: https://doi.org/10.1016/j.energy.2021.120211.
- 32. Ebeed M., Abdelmotaleb M.A., Khan N.H., Jamal R., Kamel S., Hussien A.G., Zawbaa H.M., Jurado F., Sayed K. A Modified

- Artificial Hummingbird Algorithm for solving optimal power flow problem in power systems. *Energy Reports*, 2024, vol. 11, pp. 982-1005. doi: https://doi.org/10.1016/j.egyr.2023.12.053.
- 33. Mezhoud N., Ayachi B., Amarouayache M. Multi-objective optimal power flow based gray wolf optimization method. *Electrical Engineering & Electromechanics*, 2022, no. 4, pp. 57-62. doi: https://doi.org/10.20998/2074-272X.2022.4.08.
- 34. Jamal R., Khan N.H., Ebeed M., Zeinoddini-Meymand H., Shahnia F. An improved pelican optimization algorithm for solving stochastic optimal power flow problem of power systems considering uncertainty of renewable energy resources. *Results in Engineering*, 2025, vol. 26, art. no. 104553. doi: https://doi.org/10.1016/j.rineng.2025.104553.
- 35. Hassan M.H., Kamel S., Alateeq A., Alassaf A., Alsaleh I. Optimal Power Flow Analysis With Renewable Energy Resource Uncertainty: A Hybrid AEO-CGO Approach. *IEEE Access*, 2023, vol. 11, pp. 122926-122961. doi: https://doi.org/10.1109/ACCESS.2023.3328958.
- **36.** Laifa A., Ayachi B. Application of whale algorithm optimizer for unified power flow controller optimization with consideration of renewable energy sources uncertainty. *Electrical Engineering & Electromechanics*, 2023, no. 2, pp. 69-78. doi: https://doi.org/10.20998/2074-272X.2023.2.11.
- *37.* Nagarajan K., Rajagopalan A., Bajaj M., Raju V., Blazek V. Enhanced wombat optimization algorithm for multi-objective optimal power flow in renewable energy and electric vehicle integrated systems. *Results in Engineering*, 2025, vol. 25, art. no. 103671. doi: https://doi.org/10.1016/j.rineng.2024.103671.
- 38. Nassef A.M., Abdelkareem M.A., Maghrabie H.M., Baroutaji A. Review of Metaheuristic Optimization Algorithms for Power Systems Problems. *Sustainability*, 2023, vol. 15, no. 12, art. no. 9434. doi: https://doi.org/10.3390/su15129434.
- 39. Mohamed A.A., Kamel S., Hassan M.H., Domínguez-García J.L. Optimal Power Flow Incorporating Renewable Energy Sources and FACTS Devices: A Chaos Game Optimization Approach. *IEEE Access*, 2024, vol. 12, pp. 23338-23362. doi: https://doi.org/10.1109/ACCESS.2024.3363237.
- 40. Nguyen T.T., Nguyen H.D., Duong M.Q. Optimal Power Flow Solutions for Power System Considering Electric Market and Renewable Energy. *Applied Sciences*, 2023, vol. 13, no. 5, art. no. 3330. doi: https://doi.org/10.3390/app13053330.
- 41. Gurumoorthi G., Senthilkumar S., Karthikeyan G., Alsaif F. A hybrid deep learning approach to solve optimal power flow

- problem in hybrid renewable energy systems. *Scientific Reports*, 2024, vol. 14, no. 1, art. no. 19377. doi: https://doi.org/10.1038/s41598-024-69483-4.
- 42. Adhikari A., Jurado F., Naetiladdanon S., Sangswang A., Kamel S., Ebeed M. Stochastic optimal power flow analysis of power system with renewable energy sources using Adaptive Lightning Attachment Procedure Optimizer. *International Journal of Electrical Power & Energy Systems*, 2023, vol. 153, art. no. 109314. doi: https://doi.org/10.1016/j.ijepes.2023.109314.
- 43. Laouafi F. Improved grey wolf optimizer for optimal reactive power dispatch with integration of wind and solar energy. *Electrical Engineering & Electromechanics*, 2025, no. 1, pp. 23-30. doi: https://doi.org/10.20998/2074-272X.2025.1.04.
- 44. Bai J., Nguyen-Xuan H., Atroshchenko E., Kosec G., Wang L., Abdel Wahab M. Blood-sucking leech optimizer. *Advances in Engineering Software*, 2024, vol. 195, art. no. 103696. doi: https://doi.org/10.1016/j.advengsoft.2024.103696.
- **45.** MATPOWER. Free, open-source tools for electric power system simulation and optimization. Available at: https://matpower.org/about/ (accessed on 27 April 2024).
- **46.** Bouhadouza B., Bouktir T., Bourenane A. Transient Stability Augmentation of the Algerian South-Eastern Power System including PV Systems and STATCOM. *Engineering, Technology & Applied Science Research*, 2020, vol. 10, no. 3, pp. 5660-5667. doi: https://doi.org/10.48084/etasr.3433.
- 47. Kennedy J., Eberhart R. Particle swarm optimization. *Proceedings of ICNN'95 International Conference on Neural Networks*, 1995, vol. 4, pp. 1942-1948. doi: https://doi.org/10.1109/ICNN.1995.488968.
- **48.** Mirjalili S., Mirjalili S.M., Lewis A. Grey Wolf Optimizer. *Advances in Engineering Software*, 2014, vol. 69, pp. 46-61. doi: https://doi.org/10.1016/j.advengsoft.2013.12.007.

Received 06.06.2025 Accepted 16.08.2025 Published 02.11.2025

B. Bouhadouza¹, Senior Lecturer,

F. Sadaoui¹, Professor,

¹Department of Electrical Engineering, Faculty of Applied Sciences, University of Kasdi Merbah Ouargla, Algeria,

e-mail: bouhadouza.boubekeur@univ-ouargla.dz

(Corresponding Author); sadaoui.fares@univ-ouargla.dz

How to cite this article:

Bouhadouza B., Sadaoui F. Optimal power flow analysis under photovoltaic and wind power uncertainties using the blood-sucking leech optimizer. *Electrical Engineering & Electromechanics*, 2025, no. 6, pp. 15-26. doi: https://doi.org/10.20998/2074-272X.2025.6.03